Macrocell corrosion in carbonated Portland and Portland-fly ash concrete - contribution and mechanism

Andres Belda Revert[1], Karla Hornbostel[2], Klaartje De Weerdt[1], Mette Rica Geiker[1]

[1]*Norwegian University of Science and Technology. Department of Structural Engineering.*
andres.b.revert@ntnu.no

[2]*Norwegian Public Road Administration (Statens vegvesen), Trondheim, Norway*

Abstract

The corrosion of reinforcement in carbonated concrete with high moisture state was measured with and without electrical connection to reinforcement in non-carbonated concrete. The impact of the fly ash content and the cathode-to-anode ratio (C/A) was studied. A model was proposed and applied to quantify the contribution of the anodic, cathodic and ohmic partial processes to the macrocell corrosion and the impact of C/A.

The total current density for the high moisture state investigated was high in all cases regardless the amount of fly ash replacement. The governing partial process depended on the cathode-to-anode ratio.

Keywords:

C. Carbonation

C. Corrosion

D. Blended cement

D. Fly ash

E. Concrete

Nomenclature/definitions:

Microcell (uniform) corrosion: the corrosion process in which the anodic and cathodic sites are randomly distributed and continuously alternating. The oxidation of the metal and reduction of oxygen (or hydrogen) take place in adjacent places on the same metal part.

Macrocell (galvanic) corrosion: the corrosion process in which the oxidation of the metal and reduction of oxygen (or hydrogen) take place in defined and spatially separated places that can be either on the same metal part or on two different metal parts that are electrically connected.

AC-EIS (EIS): alternating electrochemical impedance spectroscopy

C/A: cathode-to-anode area ratio [-]

CE: counter electrode

i: current density [$\mu A/cm^2$]

i_g: macrocell (galvanic) current density in the active electrode of the macrocouple [$\mu A/cm^2$]

I_g: galvanic current intensity [μA]

i_{mi-A}: microcell current density when there is no macrocouple [$\mu A/cm^2$]

i_{mi-A+C}: microcell current density in the active electrode of the macrocouple [$\mu A/cm^2$]

i_{tot}: total current density (microcell and macrocell) [$\mu A/cm^2$]

LPR: linear polarization resistance

m_{A-an}: activation control slope for active reinforcement [mV/Dec]

m_{A-cath}: activation control slope for passive reinforcement [mV/Dec]

m_{C-an}: activation control slope for sample C anodic reaction [mV/Dec]

m_{C-cath}: activation control slope for sample C cathodic reaction [mV/Dec]

OCP: open circuit potential [mV]

PC: Portland cement

PCFA: Portland-fly ash cement

PDP: potentiodynamic polarization curve

$R_{A\text{-}C}$: electrical resistance between reinforcement in carbonated concrete and non-carbonated concrete [Ω]

RE: reference electrode

RH: relative humidity [%]

R_p: polarization resistance [Ω]

SCE: external saturated calomel reference electrode

w/c: water-to-cement ratio [-]

WE: working electrode

ZRA: zero resistance ammeter

ΔE_A: anodic polarization of active steel (anode) when coupled with passive steel [mV]

$\Delta E_{A\text{-}C}$: difference in potential between active and passive steel when coupled (ohmic drop) [mV]

ΔE_C: cathodic polarization of passive steel when coupled with active steel [mV]

ρ: electrical resistivity of concrete [Ω·m]

1. Introduction

Carbonation is the spontaneous reaction of CO_2 with cement-based materials. Reinforcement embedded in sound concrete is covered with a thin oxide layer, which protects the reinforcement from further corrosion [1]. Once the carbonation front reaches the reinforcement and the concrete-steel interface is carbonated, active corrosion can develop [2].

Substitutions of Portland cement with supplementary cementitious materials are known to reduce the carbonation resistance of concrete. This is e.g. taken into account in the Norwegian standard NS-EN 206 [3]. According to the NS-EN 206 [3], the w/c is limited to maximum 0.60 for CEM I and 0.50 for CEM II/B-V, while CEM II/B-M cannot be used for concretes in the M60 Norwegian durability class (M60 corresponds to exposure classes XC3 and XC4 in EN-1992 [4]).

The corrosion process of steel embedded in concrete comprises four complementary processes: the oxidation of iron at the anodic site, the reduction of oxygen or hydrogen at the cathodic site, the transport of electrons through the reinforcement, and the transport of ions through the concrete. At any given time, the most restrictive process controls the overall corrosion process. [1] Microcell corrosion occurs when the anodic and cathodic reactions take place randomly at neighbouring sites on the same metal part [5]. Macrocell corrosion takes place when the anodic sites are spatially separated from the cathodic sites.

Carbonation is assumed to lead to microcell corrosion in the depassivated fraction of the reinforcement. However, parts of the reinforcement will remain passive due to the spatial variation of the carbonation front [2], or the reinforcement layout. This leads to macrocell corrosion in addition to microcell corrosion [1].

Slightly higher microcell current density were reported for steel embedded in carbonated concrete or mortar with Portland-fly ash cement (PCFA) than with Portland cement (PC), see Section 2.1. For Portland cement concrete, the contribution of macrocell corrosion can be significant; see Section 2.2. No information is available on the impact of fly ash on carbonation-induced macrocell corrosion.

In the current investigation, we studied corrosion (microcell and macrocell) in carbonated concrete with varying fly ash content (0, 18 or 30%) and cathode-to-anode ratios (C/A)). The hypothesis was that fly ash addition could limit the contribution of macrocell corrosion due the reported higher electrical resistivity of non-carbonated concrete with PCFA compared to PC [1].

Reinforcement embedded in carbonated concrete varying in fly ash content was electrically connected to reinforcement embedded in non-carbonated concrete and kept at a high moisture state (≈100% RH). The cathode-to-anode ratio (C/A) was either 1.6 or 5.0. The microcell and macrocell corrosion was studied by measuring electrochemical parameters. A model was proposed and applied to quantify the contribution of the anodic, cathodic and ohmic partial processes to the macrocell corrosion and the impact of C/A on the contribution of the macrocell. The relevance of the results for service life design and assessment of existing structures is briefly discussed.

2. Background

2.1. Microcell corrosion in carbonated Portland and Portland-fly ash concrete

Results in the literature indicate slightly higher microcell current density for steel embedded in carbonated concrete or mortar with PCFA than with PC when exposed to the same environment [6-10]. Figure 1 summarizes our literature review of documented current densities in various exposure conditions, including the average, maximum and minimum values reported in each investigation reviewed. The following paragraphs give a summary of the investigations.

Alonso et al. [6] investigated mortar samples (w/c 0.50) containing PC and PCFA (30% FA) among other cements. They prepared 20x55x80 mm mortar samples and cured them for 28 days at 100% RH. The samples were carbonated at 50-70% RH in a high CO_2 concentration (not specified). The carbonated samples were exposed to cycles varying between 100% RH, 50% RH, and partial immersion. The microcell current density was determined using Linear Polarization Resistance (LPR) using positive feedback for the ohmic drop compensation. Their measurements were non-conclusive.

Dhir et al. [7] prepared a series of concretes varying in w/c (0.35-0.66) and fly ash replacement (26%-36% by mass). They prepared 100 mm reinforced concrete cubes with embedded steel (ribbed carbon steel with diameter 10 mm and concrete cover 25 mm). The cubes were cured for 28 days immersed in water or directly exposed to air at 55% RH. Then the cubes were exposed to accelerated carbonation (55% RH, 4% CO_2) until the carbonation front reached 35 mm. Carbonation development was monitored in complementary plain samples. The carbonated cubes were exposed for 20 weeks to various exposure conditions: 55%, 75% or 95% RH or 55-95% RH cycles. The corrosion rate was determined using LPR (Sycopel potentiostat) with automatic ohmic drop compensation. The microcell current density in the PCFA samples was slightly higher than in the PC samples.

Arachchige [8] prepared 100 mm reinforced concrete cubes (w/c 0.55) containing PC and PCFA (30% FA) and varying amounts of cement and of fine and coarse aggregates. Embedded steel (ribbed carbon steel with diameter 10 mm and concrete cover 25 mm) was used. The cubes were preconditioned for 28 days at 55% RH and subsequently exposed to carbonation (55% RH, 4% CO_2) until the carbonation front was 35 mm. Finally, the cubes were exposed to 95% RH for 24 weeks. The corrosion rate was determined using LPR with automatic ohmic drop compensation. The microcell current density measured at 95% RH was higher in the PCFA samples than in PC samples.

Zornoza et al. [9] prepared 20x60x80 mm mortar samples (w/c 0.40) containing PC and PCFA (30% FA) including two 8 mm reinforcement bars with 6 mm of cover. The samples were cured for 80 days at 100% RH and then exposed to carbonation at 65% RH and 100% CO_2. Once carbonated, they were kept at 100% RH. The corrosion rate was determined by LPR using a potentiostat-galvanostat (EG&G PAR Model 362). No information is given on how the ohmic drop was compensated. The microcell current density measured in the PCFA samples was similar to the current density in the PC samples, but lower values were reported than in other investigations.

Messina et al. [10] prepared reinforced concrete samples (w/c 0.55) containing PC and PCFA (18% or 30% FA). They used ribbed carbon steel diameter 16 mm, and the concrete cover was 20 mm. The samples were sealed cured for two weeks and then exposed to high CO_2 concentration (5% for 10 months and ≈100% until fully carbonated (detected using pH indicator thymolphthalein)). The samples were exposed

to wetting–drying cycles while monitoring the current density for ca. 2 months. The current density was determined using non-compensated LPR, and the ohmic drop was determined using EIS. The microcell current density measured in the PCFA samples was slightly higher than in PC samples.

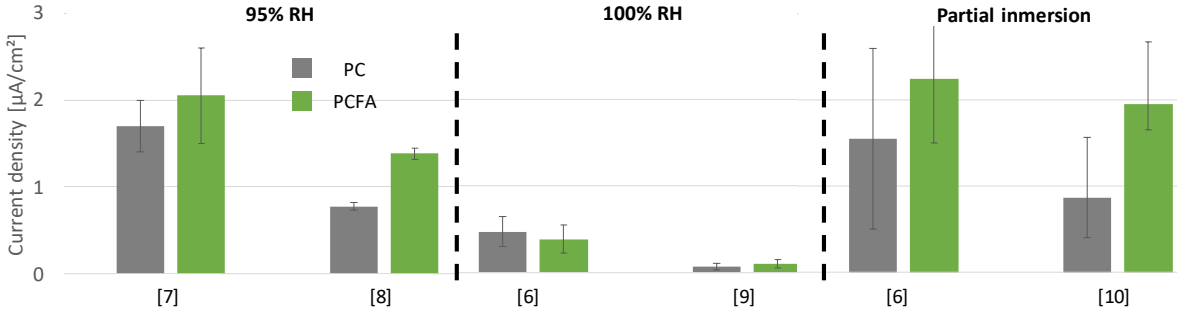

Figure 1: Microcell current density of carbon steel embedded in carbonated cementitious materials containing PC (grey bars) and PCFA (green bars) in three different exposure conditions (RH 95%, 100%, or partial immersion). Average (bars) and range (error bars). The number in brackets indicates the reference. After [6-10]

2.2. Macrocell corrosion in carbonated concrete

The literature provides no results on the influence of fly ash on macrocell corrosion in carbonated concrete. Thus, the literature review given here focuses on macrocell corrosion in carbonated concrete prepared with plain Portland cement.

Castel et al. [11-13] investigated galvanic corrosion in reinforcement embedded in carbonated PC concrete coupled with reinforcement embedded in non-carbonated PC concrete. They prepared reinforced concrete samples (w/c 0.45) containing reinforcement bars (diameter 12 mm) either as-received or cleaned (mill scale removed), and with or without casting defects in the concrete-steel interface (owing to so-called top-bar effect [14]). The carbonated samples were coupled with the non-carbonated samples with half of their height immersed in water. The current between the samples was monitored using a zero-resistance ammeter (ZRA). The distance between the reinforcement bars was 60 mm, and both C/A=2.0 and C/A=5.0 were tested. The microcell activity was determined in complementary fully carbonated samples using LPR, compensating for ohmic drop using EIS. Castel et al. found that the macrocell current density was higher than the microcell current density in the materials and conditions tested. They measured a microcell current density of ca. 0.5 µA/cm^2, a macrocell current density of 0.9 µA/cm^2 for C/A=2.0, and of 1.3 µA/cm^2 for C/A=5.0 in samples with reinforcement as-received and without casting defects in the concrete-steel interface.

Sohail et al. [15] investigated macrocell corrosion between reinforcement embedded in carbonated PC concrete and reinforcement embedded in non-carbonated PC concrete. First, they carbonated a concrete cylinder (diameter 65 mm) containing a carbon steel bar diameter 20 mm. The carbonated sample was cast into new concrete, placed in the middle of a cylindrical mould with four carbon steel bars (diameter 20 mm) reinforcement bars concentrically placed around it with 65 mm distance. The samples were kept with half their height immersed in water during the measurements. Sohail et al. measured galvanic currents, using a ZRA when coupling 1, 2, 3 or all 4 bars (C/A 1 to 4) and determined macrocell current densities from 0.7 to 4.0 µA/cm² depending on the C/A. Microcell activity was not determined in this investigation, but the results show that the macrocell contribution may not be negligible.

3. Experimental

Reinforced concrete samples were prepared and fully carbonated in a previous investigation [10]. In the following, these samples are referred to as “A samples”, indicating active corrosion. In addition, non-carbonated reinforced concrete samples with three reinforcing bars were prepared. These samples offered additional cathode when macrocoupled with the A samples and are referred to as “C samples”. The same type of cements, aggregates and reinforcement were used in both types of samples, however the samples differed in age. The A samples were obtained by subdividing samples with two reinforcement bars, resulting in A samples with bars in original top and bottom position, see Figure 3.

Figure 2 presents an overview of the samples, methods and coupling conditions together with the legends used in the paper. Samples were prepared with three different cements, which are indicated with different colours: grey is used for the PC (0% FA), blue for the 18% FA, and green for the 30% FA. When the samples were coupled (A+C), two cathode-to-anode ratios were investigated: 1.6 (circle symbols) and 5.0 (square symbols). The position of reinforcement during the casting of the A samples: top (open symbol) or bottom (solid symbol)).

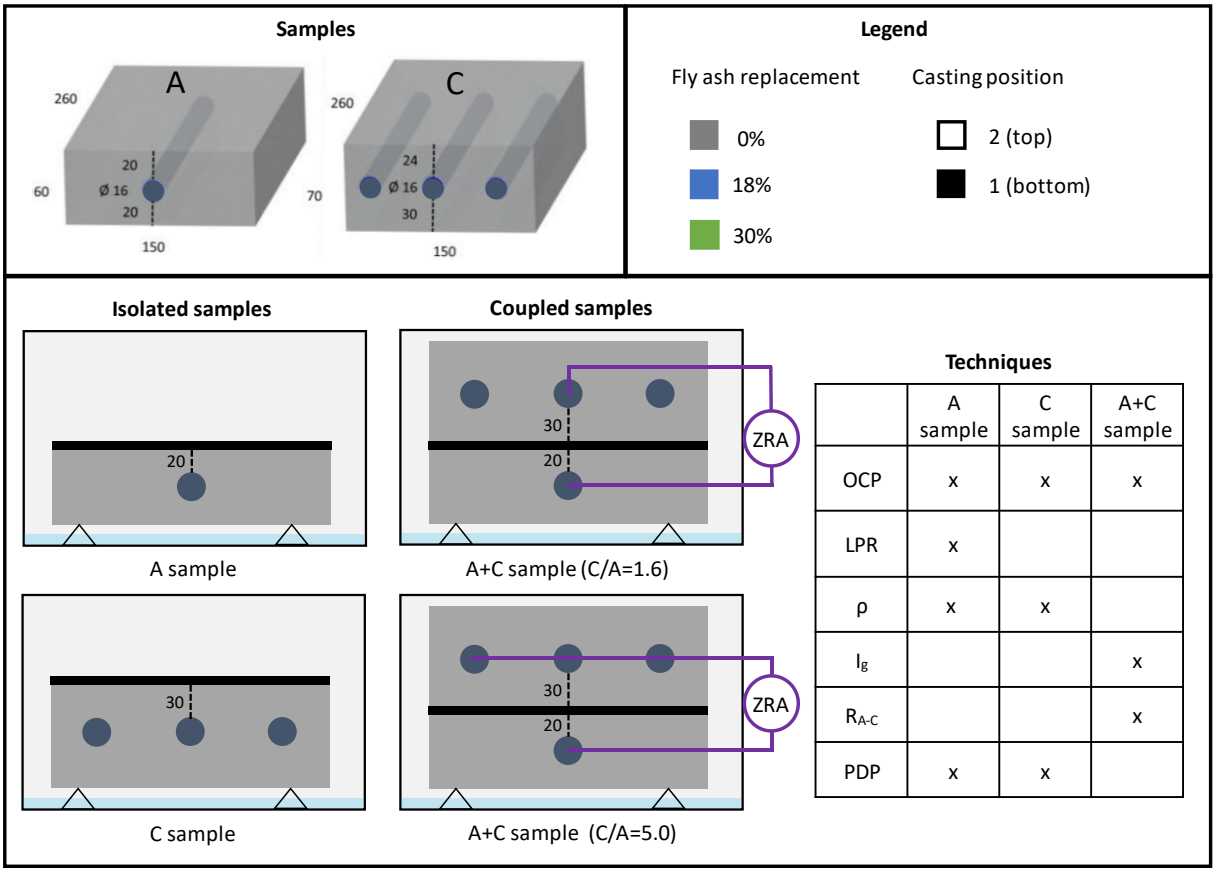

	A sample	C sample	A+C sample
OCP	x	x	x
LPR	x		
ρ	x	x	
I_g			x
R_{A-C}			x
PDP	x	x	

Figure 2: Overview of the reinforced concrete samples and methods: sample dimensions [mm] (carbonated (A) and non-carbonated (C)); legend (sample type, amount of fly ash (FA), casting position (in original sample; see Figure 3, and coupling

condition (A and C samples isolated or coupled with C/A=1.6 or C/A=5.0)); and experimental techniques. The experimental techniques are described in the text

3.1. Concrete composition

Table 1 gives the chemical composition of the three cements investigated, as determined by XRF.

Table 1: Chemical composition of the cements investigated, as determined by XRF facilitated by NORCEM AS [% by mass]

Cement	% FA	SiO_2	Al_2O_3	Fe_2O_3	CaO	MgO	SO_3	P_2O_5	K_2O	Na_2O
CEM I	0%	19.6	4.9	3.1	60.8	2.3	3.7	0.1	0.9	0.5
CEM II/B-M	18%	25.5	7.6	4.2	50.7	2.1	3.3	0.2	1.1	0.6
CEM II/B-V	30%	28.4	8.8	4.4	46.9	2.2	2.7	0.2	1.2	0.6

Concretes were prepared aiming at water-to-cement ratio (w/c) 0.55. Table 2 presents the concrete composition of the type A samples, which were cast in a precast plant in Norway, with a batch volume of 1 m^3, and the concrete composition of the type C samples, which were cast in the laboratory, with a batch volume of 7 litres.

Table 2: Concrete compositions of A and C samples [kg/m^3]. Weight of the aggregates given in saturated-surface dry condition

Constituent	A samples [kg/m^3]			C samples [kg/m^3]		
	CEM I	CEM II/B-M	CEM II/B-V	CEM I	CEM II/B-M	CEM II/B-V
Cement	371.4	369.8	369.5	376.6	376.6	376.6
Sand 0/8 mm	1173.2	1166.9	1160.3	923.2	923.2	923.2
Gravel 5/16 mm	624.2	628.5	629.6	769.2	769.2	769.2
Free water	206.9	202.9	200.9	207.2	207.2	207.2
Superplasticiser (Dyn. XTend)	3.78	3.69	3.68	-	-	-
w/c	0.56	0.55	0.54	0.55	0.55	0.55

3.2. Preparation and conditioning of A samples

The A samples were obtained by subdividing samples 150x120x260 mm in size, which were cast with two ribbed reinforcement bars 260 mm in length. Both ends of the bars were coated with beeswax to a length of 50 mm, preventing corrosion here.

The original samples were cast at a pre-cast concrete plant together with other elements. Concrete mixed at production scale was poured into the moulds and gentle compaction was applied by tapping on the sides of the mould with a rod until no air bubbles appeared on the surface. The samples were sealed cured for 14 days and subsequently carbonated at 5% CO_2, 95% RH for 10 months.

To enhance the carbonation of the samples, the original samples were cut longitudinally into two samples resulting in two types of A samples (casting position 1 (bottom) and casting position 2 (top)), see Figure 3. Subsequently, the samples were exposed to further carbonation at CO_2≈100% and 60% RH until fully carbonated (detected using pH indicator thymolphthalein)).

Probes for resistivity measurements were embedded in one of the longitudinal sides on each sample and a pseudo-reference electrode (a piece of activated titanium 25 mm in length and 1 mm in diameter) was embedded close to the reinforcement. The samples were exposed to one wetting-drying cycle as part of

another investigation [10] and kept in the laboratory until the current investigation. More details can be found in [10]. Before the current investigation, the samples were immersed in water for 4 weeks.

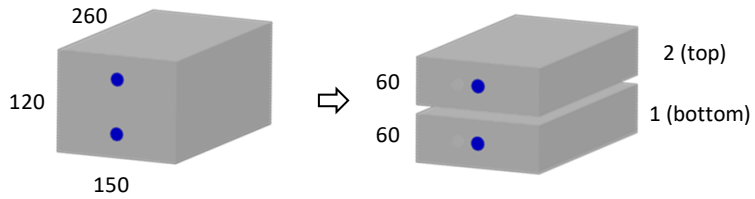

Figure 3: Sampling of A samples cast sample by longitudinal cutting cast samples. Measures in mm. After [16]

3.3. Preparation and conditioning of samples C

The C samples were cast in the laboratory. Three ribbed reinforcement bars 16 mm in diameter, 260 mm in length, were embedded in each C sample. An electrical connection was added to each bar. The reinforcement bars were separated from each other by 50 mm and by 25 mm from the edges of the sample. The concrete was poured into the moulds and gentle compaction was applied by tapping on the sides with a rod until no air bubbles appeared on the surface. The samples were sealed cured for 5 weeks at 20°C and 4 weeks at 38°C to promote the hydration of the cement and enhance differences in the electrical resistivity of the concretes. After the curing, the samples were kept over water for 3 days in a sealed plastic box before they were coupled with the A samples.

3.4. Exposure and experimental setup

During the experimental period, the samples (both A and C) were kept over water in closed boxes (corrosion current measurements show that the samples were not oxygen depleted during the investigation). At the start of the investigation, the A samples were 2 years old, while the C samples were 9 weeks old.

To ensure electrical contact between the samples, a piece of wet cloth was placed as illustrated in Figure 2 (thick black line). The temperature varied between 18 and 22 °C, and the RH in the boxes was close to 100%. The distance between the reinforcement bars embedded in the A and C samples was approximately 50 (±5) mm.

Two cathode-to-anode configurations were investigated: 1) the middle bar from the C samples connected to the bar from the A samples (C/A=1.6), and 2) all the three bars from the C samples connected to the bar from the A samples (C/A=5.0); see Figure 3.

3.5. Methods

A diagrammatic summary of the experimental techniques used on each sample is presented in Figure 2. A description of each technique is given in the following text.

The open circuit potential (OCP) was measured on A and C samples before they were coupled, and at regular intervals after coupling. The OCP of the reinforcement was measured using an external saturated calomel reference electrode (SCE) and a high impedance voltmeter (Fluke 76, input impedance 10 MΩ).

When the samples were not coupled, the SCE was placed in the middle of the reinforcement on the concrete surface. When coupled, the SCE was placed on one of the sides of the samples equidistant from the reinforcement embedded in carbonated and in non-carbonated concrete. The measurement was performed every day for C/A=5.0 and occasionally for C/A=1.6.

Before the coupling the microcell corrosion in the A samples was determined using linear polarization resistance (LPR). The polarization resistance of the reinforcement was determined using LPR using the embedded pseudo-reference electrode (RE) and a titanium mesh applied to the concrete surface as counter electrode (CE). The reinforcement (WE) was polarized ±10 mV from the OCP at a rate of 0.167 mV/min. The ohmic drop between the RE and WE was determined using AC electrochemical impedance spectroscopy (EIS) applying an alternating sinusoidal voltage of 10 mV in the range of 500 kHz to 1 Hz. The microcell current density was calculated using the Stern-Geary equation [17] assuming B=26 mV [18].

The electrical resistivity of the concrete (ρ) in the A samples was determined from the ohmic drop between the WE and RE (same setup as used for LPR). The cell factor of this corrosion cell was empirically determined from the data retrieved in a previous investigation [10]. The electrical resistivity of the concrete in the C samples was determined using EIS with each of the two neighbouring reinforcement bars as electrodes. An alternating sinusoidal voltage of 10 mV in the range of 500 kHz to 1 Hz was applied and the resistance associated with the lowest phase angle of the Bodo plot was attributed to the electrical resistance of the concrete. The cell factor of each sample was empirically determined using an electrolyte of known conductivity before the concrete was cast.

The electrical resistance ($R_{A\text{-}C}$) between the reinforcement bars embedded in the A and C samples was determined using EIS. An alternating sinusoidal voltage of 10 mV in the range of 500 kHz to 1 Hz was applied and the resistance associated with the lowest phase angle of the Bodo plot was attributed to the electrical resistance of the concrete. The resistance between the reinforcement in the C and A samples was determined before macrocoupling and after disconnecting them.

The macrocell (galvanic) current (I_g) flowing between the reinforcement embedded in carbonated and non-carbonated concrete was measured using a ZRA.

Potentiodynamic polarization curves (PDPs) were performed on A and C samples. An SCE applied on the concrete surface was used as RE, a titanium mesh applied on the opposite concrete surface as CE, and the reinforcement as WE. The reinforcement was polarized at a rate of 1 mV/s, step height 1 mV (ohmic drop non-compensated), first cathodically, and once back to the OCP, anodically. The C samples (with 3 reinforcement bars electrically connected) were polarized from -500 mV to + 250 mV vs. the OCP, while the A samples were polarized from -400 mV to + 200 mV vs. the OCP. The ohmic drop was determined using the same procedure as for LPR.

4. Results

4.1. Electrical resistivity of concrete and electrical resistance between electrodes

The electrical resistivity (ρ) of the carbonated and non-carbonated concrete was determined before macrocoupling, see Figure 4. Figure 5 presents the electrical resistance between the reinforcement bars

(electrodes) embedded in the A and C samples (R_{A-C}) right before the electrical connection was established and right after disconnection of the rebars (after 10 days of connection). The electrical resistance between the electrodes did not change during this period, which indicates that there were limited changes in the moisture state of the samples during the coupling.

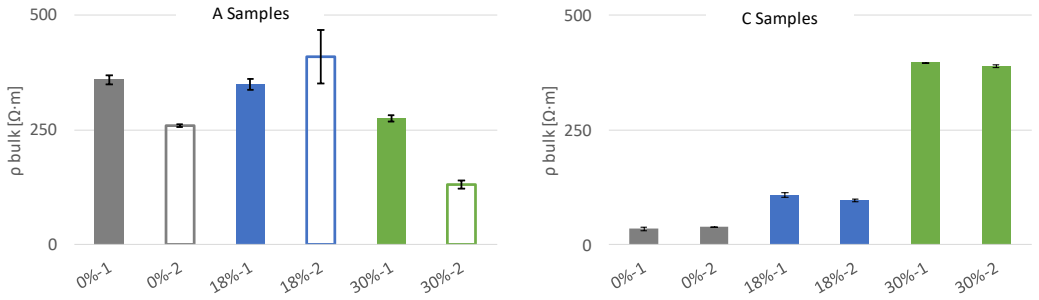

Figure 4: Electrical resistivity of concrete (ρ) measured before coupling for the carbonated A samples and the non-carbonated C samples. The samples varied in fly ash content (0, 18, 30%) and casting position of A samples (1: bottom; 2: top). Average (bars) and range (error bars)

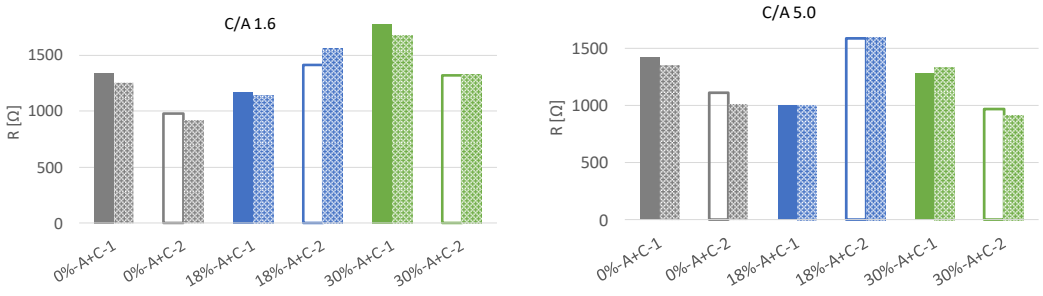

Figure 5: Electrical resistance measured between reinforcement embedded in A and C samples (R_{A-C}) before macrocoupling (solid and non-filled) and after disconnection (pattern). Left: C/A=1.6. Right: C/A=5.0. The samples varied in fly ash content (0, 18, 30%) and casting position of A samples (1: bottom; 2: top)

4.2. Potentiodynamic polarization curves

Figure 6 presents the polarization curves measured for the A samples (rebar area≈80 cm^2) and the C samples (the three reinforcement bars connected, area≈400 cm^2). Lines were fitted to the linear parts of the polarization curves. The data are summarized in Table 3. The values are not necessarily the Tafel slopes of the anodic and cathodic reactions, because they were taken in a higher polarization range than the range in which Tafel slopes are usually calculated based on the polarization due to the macrocoupling. The results were used for modelling the macrocell corrosion process.

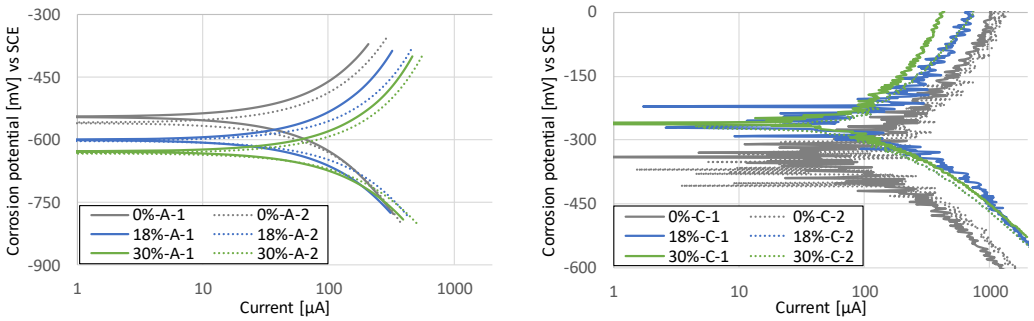

Figure 6: Potentiodynamic polarization curves for samples varying in fly ash content (0, 18, 30%) and casting position of A-samples (1: bottom; 2: top). Left: A samples (carbonated, area≈ 80 cm²). Right: C samples (non-carbonated, area ≈ 400 cm²)

Table 3: Activation control slopes derived from the PDP (slope of regression lines assuming activation control) [mV/Dec]

Samples	Slope of the linear part of the polarization curves	Fly ash content		
		0 %	18 %	30 %
A (carbonated)	$m_{A\text{-}cath}$	340	330	290
	$m_{A\text{-}cath}$	360	360	320
C (non-carbonated)	$m_{C\text{-}an}$	8000	6000	7000
	$m_{C\text{-}cath}$	260	280	280

4.3. Microcell corrosion

The microcell current density was determined for the A samples before coupling, see Figure 7. The data includes daily measurements over four consecutive days before the coupling.

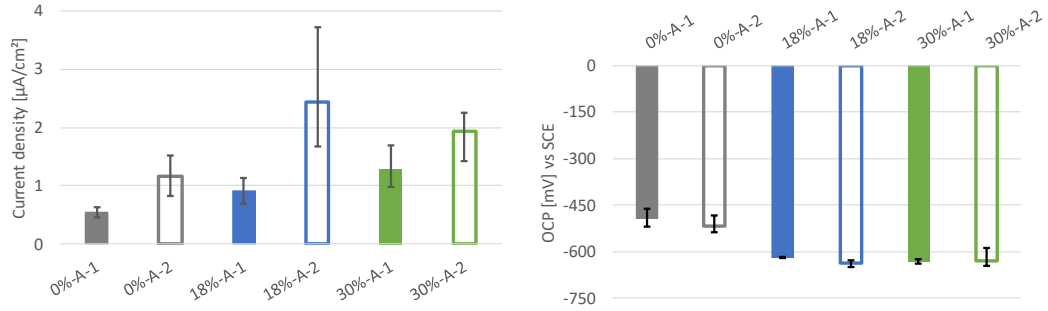

Figure 7: State of reinforcement in A samples before macrocoupling. Left: microcell current density. Right: OCP. Average (bars) and range (error bars) of 4 measurements taken on consecutive days. The samples varied in fly ash content (0, 18, 30%) and casting position of A samples (1: bottom; 2: top)

4.4. Macrocell corrosion

Figure 8 gives a summary of the OCP results before the A and C samples were coupled, and 10 days after coupling them (A+C). Figure 9 shows the galvanic (macrocell) current and the OCP of the macrocouples over time (C/A=5.0). Figure 10 presents the macrocell current densities determined after 10 days of coupling for C/A=1.6 (left) and for C/A=5.0 (right).

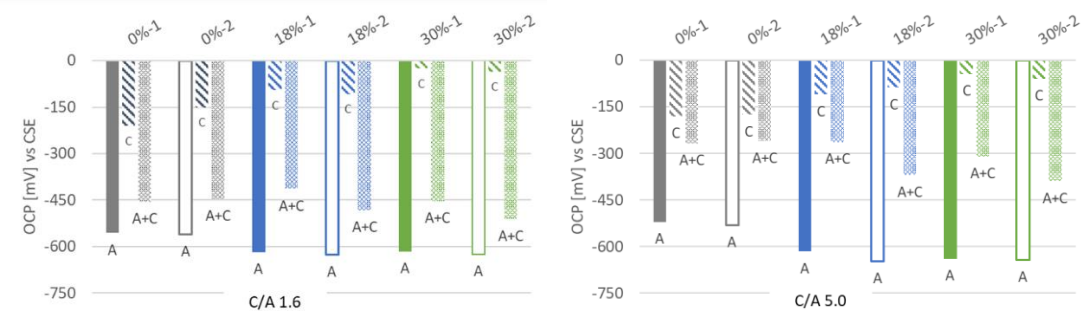

Figure 8: OCP of A samples (solid or non-filled) and C samples (stripes) before coupling and of A+C samples (pattern) after 10 days of coupling. Left: C/A=1.6. Right: C/A=5.0. The samples varied in fly ash content (0, 18, 30%) and casting position of A samples (1: bottom; 2: top)

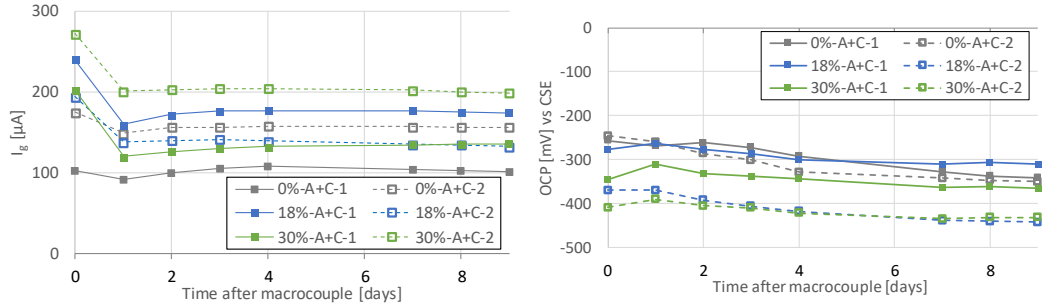

Figure 9: State of reinforcement over time in A samples after macrocoupling (C/A=5.0). Left: the galvanic (macrocell) current (I_g) . Right: OCP. The samples varied in fly ash content (0, 18, 30%) and casting position of A samples (1: bottom; 2: top)

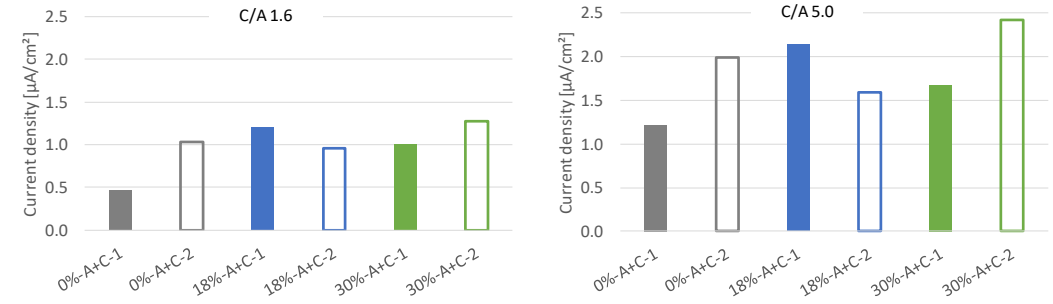

Figure 10: Macrocell current density over time 10 days after macrocoupling. Left: C/A=1.6. Right: C/A=5.0. The samples varied in fly ash content (0, 18, 30%) and casting position of A samples (1: bottom; 2: top)

5. Discussion

The corrosion of reinforcement in carbonated concrete with high moisture state was measured with and without electrical connection to reinforcement in non-carbonated concrete. The impact of fly ash content[1] and the cathode-to-anode ratio (C/A) on macrocell corrosion is the focus of the discussion. In addition,

[1] It should be noted that the performance of fly ash blends is compared to Portland cement concretes using the same water-to-cement ratio (w/c), which is not according to the NS-EN 206 [3]

microcell corrosion rates and observation on the impact of casting direction are discussed. Finally perspectives for service life design are briefly addressed.

Throughout the discussion the observed corrosion rates are assessed using the classification of severity suggested by Andrade et al. [19], see Table 4.

Table 4: Ranges of corrosion rates in reinforcement embedded in concrete according to [19]

	Severity				
	Negligible	Low	Moderate	High	Very high
Corrosion rate [µA/cm^2]	≤ 0.1	0.1-0.5	0.5-1	1-10	10-100

5.1. Microcell corrosion in carbonated concrete

The microcell current density range measured in this investigation is in agreement with data reported in the literature and in the moderate to high range according to Table 4. Higher microcell corrosion rates were measured in the PCFA samples than in the PC samples. This is in agreement with most studies in the literature (see Figure 1).

Systematically higher microcell corrosion rates were measured in the samples cast in the top position than in samples cast in the bottom position. The OCP values were not affected by the casting position. In a previous investigation [2], we found in samples of comparable size casting position dependent microstructural defects in terms of crack patterns in the vicinity of the reinforcement. Such defects may have changed the local conditions at the anode and influenced the corrosion process. However, the observation of position independent OCPs questions the assumption. Due to ongoing experiments, the samples have not been opened to verify the assumption of microstructural defects in samples A-2. The impact of casting position on current density was in the present investigation comparable to the observed impact of the binder composition.

5.2. Macrocell corrosion in carbonated concrete

5.2.1 Mechanism

The mechanism of macrocell corrosion in carbonated concrete has been described by Bertolini et al. [1] and Castel et al. [12] amongst others. Below we describe the macrocell mechanism using parameters that can be experimentally retrieved.

Figure 11 uses Evans diagrams to present a simplified model, which illustrates the influence of coupling active reinforcement embedded in carbonated concrete (an A sample) with passive reinforcement embedded in non-carbonated concrete (a C sample). The vertical axis is the corrosion potential (E_{corr}), and the horizontal axis is the current in logarithmic scale. (The sketch presented is based on data retrieved from the investigated samples with C/A=5.0).

When the reinforcement embedded in carbonated concrete (the A sample) is coupled with reinforcement embedded in non-carbonated concrete (the C sample), the A sample is anodically polarized (ΔE_A) to more positive E_{corr} values, while the C sample is cathodically polarized (ΔE_C) to more negative E_{corr} values. According to this simplified model, there is a difference in potential between the active and passive

reinforcement ($\Delta E_{A\text{-}C}$) which equals to the electrical resistance ($R_{A\text{-}C}$) between them times the current flowing (I_g). The equilibrium of the macrocell depends on the anodic and cathodic polarization curves of the two samples. The oxidation current in the C sample is almost constant (practically a vertical line), while the oxidation current in the A increases with the anodic polarization. It is possible to maintain this higher oxidation rate due to the additional reduction of oxygen in the C sample. Figure 11 illustrates how the microcell current density is affected by the coupling.

This model together with the PDPs measured (cf. Figure 6) make it possible to quantify the contribution of the partial processes involved in macrocell corrosion: the cathodic polarization of the C sample (ΔE_C), the difference in potential between the A and C samples ($\Delta E_{A\text{-}C}$), and the anodic polarization of the A sample (ΔE_A). Moreover, we can investigate local changes in the A sample due to the anodic polarization: the decrease in microcell current density (due to the lower reduction of oxygen in the A sample) and the increase in total current density (due to the galvanic couple).

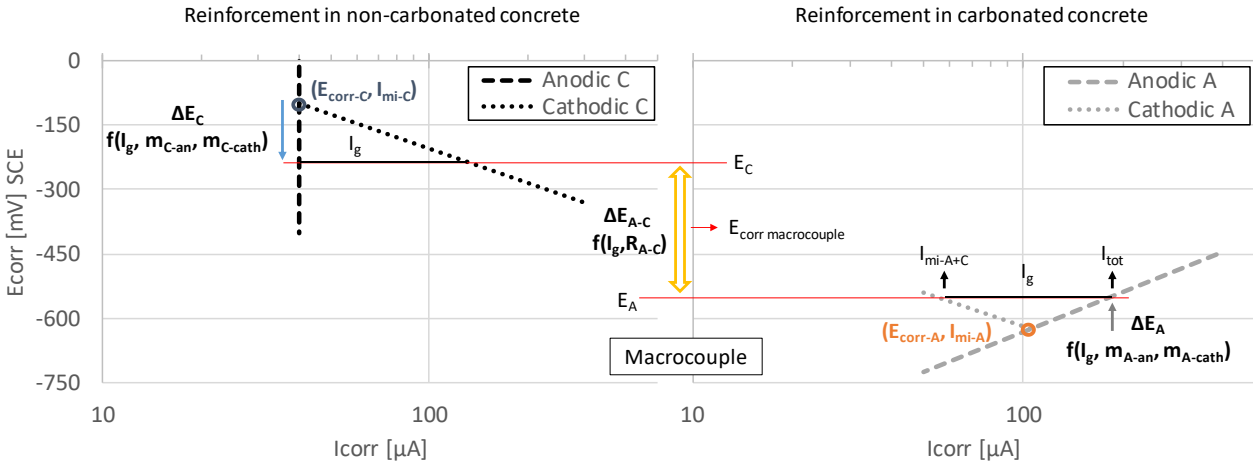

Figure 11: Proposed schematic representation of macrocell corrosion between reinforcement embedded in non-carbonated concrete (passive) and reinforcement embedded in carbonated concrete (active) based on Evans diagrams. The sketch presented here is based on experimental data for C/A=5.0

5.2.2 Macrocell contribution

As expected, the macrocell current densities increased with increased C/A. The macrocell current densities were in the moderate to high range for C/A=1.6 and in the high range for C/A=5.0 according to Table 4. Castel et al. [11-13] reported similar ranges for PC samples with C/A=2.0 and C/A=5.0 and comparable moisture state. Sohail et al. [15] determined macrocell current densities from 0.7 to 4.0 µA/cm² depending on the C/A (varied from 1 to 4). In real structures, much larger C/A and thus a larger contribution of macrocell corrosion might be expected; this is further discussed in Section 5.2.4.

Figure 12 illustrates the microcell corrosion current density determined in the A samples before coupling ($i_{mi\text{-}A}$), and the total current density (i_{tot}) determined from the galvanic current (i_g) and the calculated microcell contribution ($i_{mi\text{-}A+C}$) (according section 5.2.1) when the A and C samples were connected. The stacked bars in Figure 12 (i_{tot}: lower bar $i_{mi\text{-}A+B}$ and upper bar i_g) take into account the local changes in the active reinforcement due to anodic polarization, as shown in Figure 11. The red dashed line indicates the threshold value for the corrosion rate being considered high according to Table 4. The total current density

is classified as high for all the cement types, casting positions, and C/A ratios tested in this study, for high moisture content investigated. The PCFA presented slightly higher total corrosion rates than the PC samples.

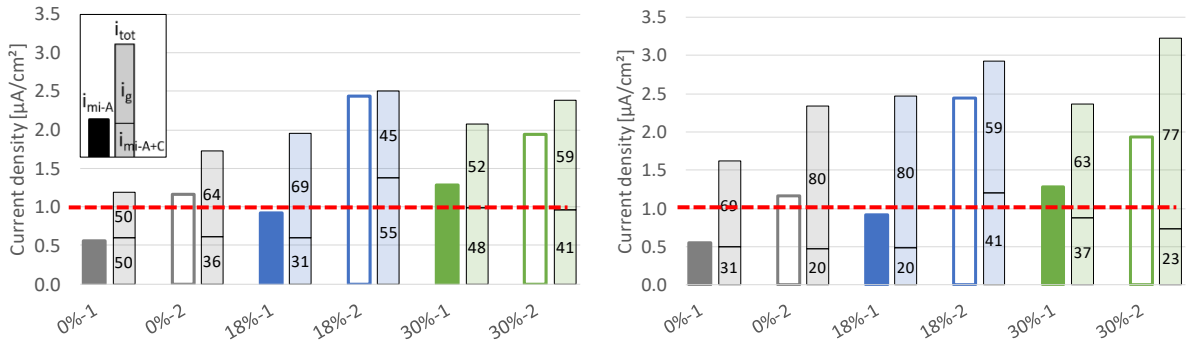

Figure 12: Microcell current density for the A samples (i_{mi-A}) two hours before coupling, and the total current density (i_{tot}) when the samples were coupled (A+C). Left: C/A=1.6. Right: C/A=5.0. The numbers in the bars show the contributions of the macrocell (i_g) and microcell (i_{mi-A+C}) as a percentage of the total current density. The red dashed line indicates the threshold for high corrosion rates according to Table 4

Figure 13 presents a comparison of the differences in potential between the A and C samples determined experimentally before they were connected (solid and non-filled bars) and the values obtained by applying the model presented in Figure 11 (shaded bars) using the electrochemical parameters presented in Table 3 for C/A=1.6 and C/A=5.0. The contribution of the three partial processes involved in the macrocell is depicted: the cathodic polarization of the C ($\Delta E_C=f(I_g, m_{C\text{-}an}, m_{C\text{-}cath})$); the difference in potential between the A and C samples ($\Delta E_{A\text{-}C}=f(I_g, R_{A\text{-}C})$); and the anodic polarization of the A ($\Delta E_A=f(I_g, m_{C\text{-}an}, m_{C\text{-}cath})$).

For C/A=1.6, the ΔE_C dissipates about 60% of the driving potential, the $\Delta E_{A\text{-}C}$ dissipates about 25%, and the remaining 15% is due to ΔE_A. ΔE_C depends on the ability of the cathode to reduce oxygen, and for C/A=1.6, it is needed higher polarization compared to C/A=5.0 to sustain the increased oxidation rate of iron in the A sample. $\Delta E_{A\text{-}C}$ becomes less relevant due to the lower galvanic current than in C/A=5.0.

For C/A=5.0, the ΔE_C dissipates about 30% of the driving potential, the $\Delta E_{A\text{-}C}$ dissipates about 50%, and the remaining 20% is due to ΔE_A. In this case, the reduction rate of oxygen can be sustained with a relatively small polarization. $\Delta E_{A\text{-}C}$ is the process which dissipates more potential due to the high galvanic current.

ΔE_A is the partial process which dissipates least potential in both cases tested (C/A=1.6 and C/A=5.0).

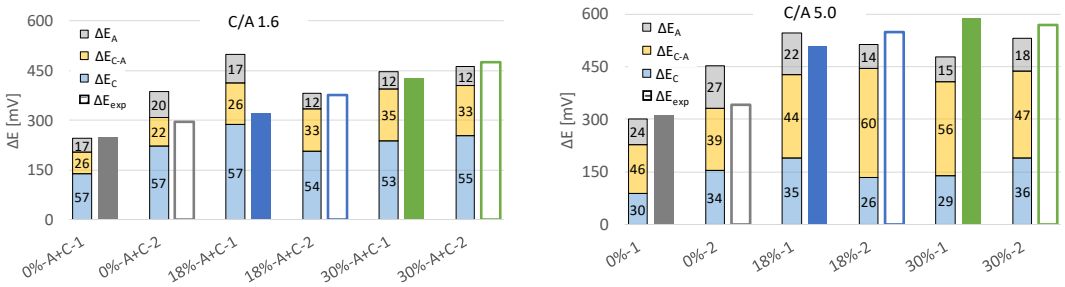

Figure 13: Calculated contribution (in percentage terms) of the three partial processes involved in macrocell corrosion (stacked bars) and measured driving potential (solid and non-filled bars). Left: C/A=1.6. Right: C/A=5.0

Figure 14 presents the relationship between the difference in potential in the carbonated and non-carbonated samples before connecting them and the macrocell current density once connected. The driving force for macrocell corrosion is the difference in potential between the active and passive steel. To make it possible to compare the results of the current investigation with the results reported by Castel et al. [11-13], their data have been treated in Figure 14 expressed in terms of current density.

Castel et al. [12] concluded that there is an exponential correlation between the macrocell driving potential and the current density that mirrors the polarization curves of the system (linear in log scale, see Figure 6). Our data set compares to their observations as illustrated in Figure 14.

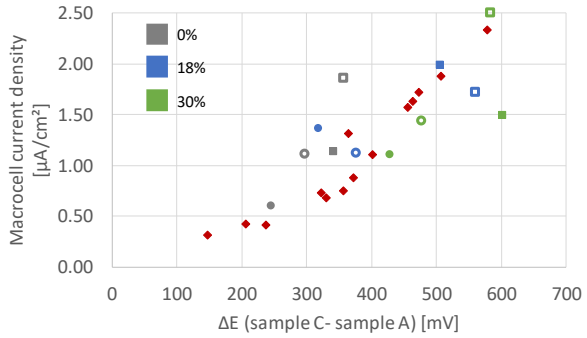

Figure 14: Relationship between the difference in the corrosion potential before coupling and the macrocell current density after coupling. Circles: C/A=1.6, squares: C/A=5.0, filled: bottom position, empty symbols: top position, red diamonds: data from [11-13]

5.2.3 Influence of fly ash content on macrocell corrosion

The hypothesis was that fly ash addition would limit the macrocell corrosion due to the higher electrical resistivity of non-carbonated PCFA concrete compared to PC concrete. However, the results illustrate a limited effect of the concrete resistivity on the corrosion process for the materials, configurations and conditions investigated. The electrical resistance between the anode and cathode in the corrosion cell tested varies only by a factor of 1.5 (see Figure 5), while the resistivity of the concretes differs 2-6 times (see Figure 4). Figure 4 presents the electrical resistivity of the concrete determined in the carbonated (A) and the non-carbonated (C) samples before they were coupled. The higher the amount of fly ash of non-carbonated concrete, the higher the electrical resistivity. In contrast, the resistivity of the carbonated PC and PCFA samples was similar. It must be noted that the electrical resistivity of the non-carbonated concrete samples cannot be directly compared with the electrical resistivity of the carbonated concrete samples due to the different age and preconditioning of the samples.

If we compare the electrical resistance in PC and PCFA (30%) samples, see Figure 5, it seems the C/A did not influence the electrical resistance determined in the PC samples. However, in the PCFA (30%) samples, the electrical resistance increased for the lower C/A. This can be explained by the electrical resistivity of the non-carbonated PCFA being higher than that of PC. The more reinforcement is embedded in non-

carbonated concrete, the higher becomes the possible beneficial influence of the fly ash in the form of higher electrical resistance. Within the range of C/A experimentally investigated this was not observed.

The driving potential between the carbonated and non-carbonated samples was higher in the PCFA samples than in the PC samples, see Figure 8 (the A samples presented more negative values while the C samples presented more positive values in the PCFA than in the PC samples). In addition, the slope of the cathodic activation control lines of the PCFA samples was slightly higher than those of the PC samples (see Table 3), which means higher current for the same polarization in the PCFA samples.

The pore solution composition of carbonated and non-carbonated PC and PCFA samples containing the same cements as used in this investigation were analysed using cold water extraction [20]. The results showed that pore solution of non-carbonated PC samples contained more alkali metal ions compared to non-carbonated PCFA. In contrast, upon carbonation PC and PCFA had similar pore solution composition. Thus, the pore solution chemistry is not expected to have influenced the corrosion process in the carbonated concrete.

The observations described above may explain the differences between expectation and observations. The results are limited to the investigated high moisture state (≈100% RH) and C/A ratios (1.6 and 5.0).

5.2.4 Influence of the cathode-to-anode ratio on macrocell corrosion

According to Table 4, the total current density is classified as high for all the samples tested in the current investigation. It is slightly higher for the PCFA samples than for the PC samples for the two C/A ratios investigated. In all cases, the 0%-1 sample gave the lowest microcell and total current density. The microcell and macrocell activity contribution is greatly influenced by the C/A. For C/A=1.6, the galvanic contribution varies in the range of 45-70% of i_{tot}, while for C/A=5.0, the galvanic contribution is about 60% to 80%. When the microcell current density before macrocoupling is compared with the total current density once connected, the ratio varies between 1.1 and 3 regardless of the amount of fly ash present.

The model presented made it possible to determine the relative influence of each of the partial processes involved in macrocell corrosion. This section discusses the influence of the cathode-to-anode ratio. In the modelling, the size of the cathode was varied while the size of the anode was fixed. In addition to C/A=5, two other cases were calculated, one low (C/A=0.5) and the other high (C/A=50), to illustrate the impact of the C/A ratio. The electrochemical parameters of the passive steel were determined from the PDPs (Figure 6) assuming they were proportional to the exposed area of reinforcement. The electrochemical parameters of the active steel were also determined from the PDPs (Figure 6). The data retrieved from the PC samples was used for this numerical application. The electrical resistance between the electrodes was assumed constant (1000 Ω), based on (Figure 5) and the discussion in [21]. Figure 15 summarizes the results.

When we compare the relative influence of the three partial processes involved in the macrocell mechanism, the higher the C/A, the more relevant becomes the ohmic partical process (difference in potential between the active and passive steel (ΔE_{A-C})). The contribution of the ohmic process appears slightly higher for PCFA than for PC. For high C/A, the data indicates support to the hypothesis that fly ash addition would limit macrocell corrosion due to the higher electrical resistivity of non-carbonated PCFA

concrete compared to PC concrete. The cathodic polarization of the passive steel (ΔE_C) is more dominant for lower C/A. The anodic polarization of the active steel (ΔE_A) seems to be independent of C/A.

The higher the C/A, the higher are the total current density and the galvanic contribution. The calculations showed that even if the active steel is coupled with a limited amount of passive steel (C/A=0.5), the macrocell effect is not negligible for this moisture condition (a factor of 1.4 when the total and uncoupled microcell current densities are compared).

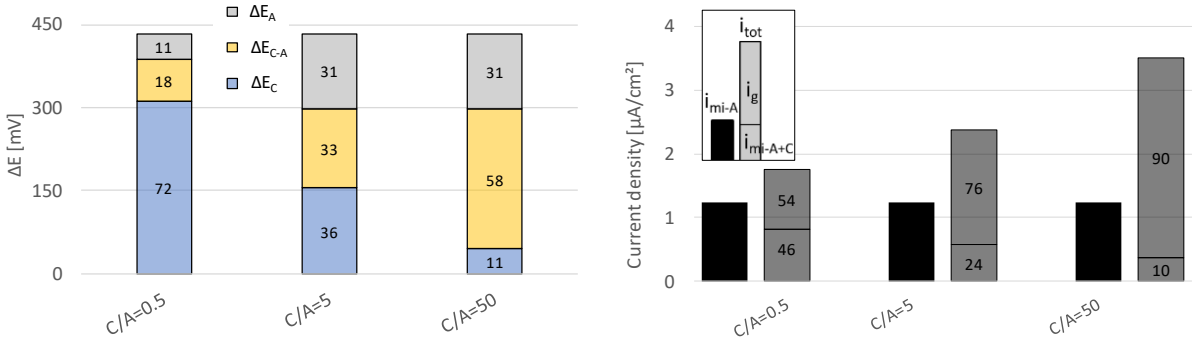

Figure 15: Left: Calculated contribution (In percentage terms) of the three partial processes involved in macrocell corrosion (stacked bars). Right: Microcell current density and calculated total current density contributions (in percentage terms)

5.3. Perspectives for service life design and reassessment of reinforced concrete structures affected by carbonation

The design service life of a reinforced concrete structure is defined as "the assumed period for which a structure or part of it is to be used for its intended purpose with anticipated maintenance, but without major repair being necessary" [22]. To quantify the service life a limit state and the level of reliability (or probability of failure) for not passing it must be selected [23]. The service life of reinforced concrete structures is usually divided into the initiation period, where a critical state is built up, and the propagation period, where damage development takes place. For reinforcement corrosion aggressive substances penetrate through the concrete cover during the initiation period, and the propagation period starts when the aggressive substances have reached the reinforcement and active corrosion occurs [24]. Once reinforcement starts to corrode actively, the remaining service life of the structure mainly depends on the corrosion rate [25]. Today, depassivation is the limit state typically used for service life design of reinforced concrete structures susceptible to corrosion, see e.g. [23]. A reliable corrosion rate estimation will support differentiation of the probability of failure and the use of other limit states. Also, corrosion rate estimations will facilitate the reassessment of existing structures.

The total current density is the value which should be considered when predicting the (residual) service life prediction, otherwise a non-conservative conclusions could be made.

The experimental and analytical data show that coupling of reinforcement in carbonated concrete to reinforcement in non-carbonated concrete polarizes the anode. This reduces the microcell activity, but increases the total corrosion rate due to macrocell activity (cf. Figure 12 and Figure 15).

In a structure, such coupling will take place on the outer reinforcement when the carbonation front passes, leading to initial high corrosion rates of first depassivated fractions of the steel (pending a high moisture state of the concrete). In addition, the outer reinforcement layer might be coupled to inner reinforcement in non-carbonated concrete leading to even higher cathode-to-anode ratios (C/A) and higher corrosion rates.

The exposure condition investigated might be considered representative of a period of wetness in a reinforced concrete structure in service. For the experimentally investigated high moisture state, the total corrosion current was high and the contribution of macrocell corrosion was substantial. The data illustrates that macrocell effects due to coupling between reinforcement in carbonated and non-carbonated concrete should be considered, both for service life design and when reassessing existing structures.

6. Conclusion

The microcell and macrocell corrosion activity of reinforcement in carbonated concrete samples was measured with and without electrical connection to reinforcement in non-carbonated samples; i.e. both microcell and macrocell corrosion were measured. The cathode-to-anode ratio (C/A) was either 1.6 or 5.0, and the samples were kept at high moisture state. Three binder compositions were used, differing in fly ash content (0%, 18% or 30%). All the concretes were prepared with the same water-to-cement ratio (0.55). A model was introduced to quantify the partial processes involved in the macrocell corrosion. The following conclusions can be drawn:

- The microcell current density in the carbonated concretes was moderate-to-high for the exposure condition tested. The microcell current density was slightly higher in the Portland-fly ash concretes than in plain Portland concrete. The impact of casting position on the microcell current density was in the present investigation comparable to the observed impact of the binder composition.
- In all cases, the macrocell current density was of the same magnitude as the microcell current density and not negligible.
- The total current density (microcell and macrocell) was high in all investigated cases and slightly higher in the Portland-fly ash concretes than in plain Portland concrete.
- The macrocell corrosion mechanism was assessed based on Evans diagrams. The contributions of the different partial processes involved in the macrocell corrosion were modelled: cathodic polarization of passive reinforcement, the difference in potential between active and passive reinforcement (ohmic process), and anodic polarization of active reinforcement. It was shown that the macrocell current depends on the C/A ratio, and that for high C/A (50) the ohmic process was the dominant partial process, whereas for low C/A (0.5) the polarization of the cathode was the dominant partial process. At C/A=5, the contribution of the three processes was comparable.
- Macrocell effects due to coupling between reinforcement in carbonated and non-carbonated concrete should be considered when making service life predictions. The exposure investigated in this study might be considered representative of a period of wetness in a field structure.

7. Acknowledgements

This project is part of a larger research project, 'Lavkarbsem' (NFR project no. 235211/O30), which is supported by the Norwegian Research Council and the following companies: Mapei AS, Norbetong AS, Norcem AS, Skanska AS, and Rambøll Engineering AS. The data was obtained partly using samples prepared in collaboration with POLIMI.

8. References

[1] L. Bertolini, B. Elsener, P. Pedeferri, E. Redaelli, R. Polder, Corrosion of Steel in Concrete, Wiley-VCH Verlag GmbH & Co, Weinheim, Germany, 2013.
[2] A. Belda Revert, K. De Weerdt, K. Hornbostel, M.R. Geiker, Carbonation-induced corrosion: Investigation of the corrosion onset, Construction and Building Materials, 162 (2018) 847-856.
[3] NS-EN 206:2013+NA:2014 Concrete, Specification, performance, production and conformity, in, Standard Norge, 2014.
[4] EN-1992, EN 1992: Design of concrete structures, in, 2004.
[5] J. Gulikers, Theoretical considerations on the supposed linear relationship between concrete resistivity and corrosion rate of steel reinforcement, Materials and Corrosion, 56 (2005) 393-403.
[6] C. Alonso, C. Andrade, J. González, Relation between resistivity and corrosion rate of reinforcements in carbonated mortar made with several cement types, Cement and Concrete Research, 18 (1988) 687-698.
[7] R.K. Dhir, M.R. Jones, M.J. McCarthy, Pulverized-fuel ash concrete: carbonation-induced reinforcement corrosion rates, Proceedings of the Institution of Civil Engineers - Structures and Buildings, 94 (1992) 335-342.
[8] A.D.M. Arachchige, Influence of cement content on corrosion resistance, Proceedings of the Institution of Civil Engineers - Construction Materials, 161 (2008) 31-39.
[9] E. Zornoza, J. Payá, P. Garcés, Carbonation rate and reinforcing steel corrosion rate of OPC/FC3R/FA mortars under accelerated conditions, Advances in Cement Research, 21 (2009) 15-22.
[10] M. Messina, A. Belda Revert, K. Hornbostel, M.R. Geiker, M. Gastaldi, Corrosion current density as a function of electrical resistivity of carbonated concrete, (In preparation).
[11] A. Castel, A. Nasser, Microcell versus galvanic corrosion currents in carbonated concrete, Magazine of Concrete Research, 66 (2014) 697-707.
[12] A. Nasser, A. Clément, S. Laurens, A. Castel, Influence of steel–concrete interface condition on galvanic corrosion currents in carbonated concrete, Corrosion Science, 52 (2010) 2878-2890.
[13] A. Castel, A. Nasser, Influence of pre-existing oxides layer and interface condition with carbonated concrete on active reinforcing steel corrosion, Materials and Corrosion, 66 (2015) 9.
[14] R. Zhang, A. Castel, R. François, Influence of steel–concrete interface defects owing to the top-bar effect on the chloride-induced corrosion of reinforcement, Magazine of Concrete Research, 63 (2011) 773-781.
[15] M.G. Sohail, S. Laurens, F. Deby, J.P. Balayssac, Significance of macrocell corrosion of reinforcing steel in partially carbonated concrete: numerical and experimental investigation, Materials and Structures, 48 (2015) 217-233.
[16] A. Belda Revert, K. Hornbostel, K. De weerdt, M.R. Geiker, Determination of the polarization resistance of steel in carbonated fly-ash concrete- effect of measurement technique, in: EUROCORR- 20th International corrosion congress-Corrosion of Steel in Concrete, Prague, 2017.
[17] M. Stern, A.L. Geary, Theoretical Analysis of the Shape of Polarization Curves, Journal of the Electrochemical Society, 104 (1957) 7.

[18] C. Andrade, V. Castelo, C. Alonso, J. González, The Determination of the Corrosion Rate of Steel Embedded in Concrete by the Polarization Resistance and AC Impedance Methods, ASTM International, (1986) 20.
[19] C. Andrade, C. Alonso, Corrosion rate monitoring in the laboratory and on-site, Construction and Building Materials, 10 (1996) 315-328.
[20] K. De Weerdt, G. Plusquellec, A. Belda Revert, M.R. Geiker, B. Lothenbach, Effect of carbonation on the pore solution of mortar, In preparation, (2018).
[21] K. Hornbostel, U.M. Angst, B. Elsener, C.K. Larsen, M.R. Geiker, On the limitations of predicting the ohmic resistance in a macro-cell in mortar from bulk resistivity measurements, Cement and Concrete Research, 76 (2015) 147-158.
[22] ISO-2394, ISO 2394: General principles on reliability for structures, in, 2015.
[23] *fib*, International Federation for Structural Concrete, *fib*, Model Code for Service Life Design, Bulletin no 34, in, Lausanne, Switzerland, 2006.
[24] K. Tuutti, Corrosion of steel in concrete, in, Swedish Cement and Concrete Research Institute, Stockholm, 1982.
[25] M. Otieno, H. Beushausen, M. Alexander, Prediction of corrosion rate in reinforced concrete structures – a critical review and preliminary results, Materials and Corrosion, 63 (2012) 777-790.